Vibrational spectroscopic studies, conformations and ab initio calculations of 2-chloroethyl trifluorosilane

ARTICLE *in* JOURNAL OF MOLECULAR STRUCTURE · JUNE 2001

Impact Factor: 1.6 · DOI: 10.1016/S0022-2860(01)00545-2

ELSEVIER

Journal of Molecular Structure 567–568 (2001) 167–185

Journal of
MOLECULAR
STRUCTURE

www.elsevier.nl/locate/molstruc

Vibrational spectroscopic studies, conformations and ab initio calculations of 2-chloroethyl trifluorosilane ☆

P. Klaeboe[a,*], C.J. Nielsen[a], V. Aleksa[a,b], A. Gruodis[a,b], G.A. Guirgis[c,1], Y.E. Nashed[c], J.R. Durig[c]

[a]*Department of Chemistry, University of Oslo, P.O. Box 1033, 0315 Oslo, Norway*
[b]*Department of General Physics and Spectroscopy, Vilnius University, Vilnius 2734, Lithuania*
[c]*Department of Chemistry, University of Missouri-Kansas City, Kansas City, MO 64110-2499, USA*

Received 7 June 2000; accepted 19 September 2000

Abstract

Infrared spectra of 2-chloroethyl trifluorosilane (CETFS) ($ClCH_2CH_2SiF_3$) were obtained in the vapour, amorphous and crystalline solid phases in the range 4000–50 cm^{-1}. Additional variable temperature spectra in liquefied xenon and spectra in argon and nitrogen matrices at 5 K were recorded. Raman spectra of the compound as a liquid were recorded at various temperatures between 298 and 180 K and amorphous and crystalline solids were obtained.

The spectra of CETFS revealed the existence of two conformers (*anti* and *gauche*) in the vapour and in the liquid. Large variations in the infrared and Raman spectra were observed when the vapour was shock-frozen on a window at 80 K and subsequently annealed. An intermediate phase appeared at ca. 125 K containing both conformers. A crystal was formed at 160 K, and ca. 18 infrared and/or Raman bands present both in the fluid phases and in the 125 K solid vanished in this crystal.

From the intensity variations between 293 and 183 K of four Raman band pairs, $\Delta H^0(anti - gauche) = 0.8 \pm 0.3$ kJ mol^{-1} was obtained in the liquid. In liquid xenon under pressure a ΔH value of -0.7 ± 0.1 kJ mol^{-1} was calculated from the intensity variations between 218 and 173 K of two band pairs in the infrared spectra. Annealing experiments indicate that the *anti* conformer has slightly lower energy in argon and nitrogen matrices. Also, the *anti* conformer has the lower energy in liquid xenon, whereas the more polar *gauche* rotamer is the low energy conformer in the liquid and is also present in the crystal. The spectra of both conformers have been interpreted in detail.

Ab initio calculations were performed using the GAUSSIAN 94 program with the HF/6-311G* basis set and gave optimized geometries, infrared and Raman intensities and scaled vibrational frequencies for the *anti* and *gauche* conformers. The conformational energy difference derived was 3.8 kJ mol^{-1} with *anti* being the low energy conformer.

Keywords: 2-Chloroethyl trifluorosilane; Vibrational spectra; Conformations; Halosilanes; Ab initio calculations

1. Introduction

2-Chloroethyl trifluorosilane ($ClCH_2CH_2SiF_3$), later to be abbreviated CETFS, was synthesized for the first time and an infrared and Raman spectroscopic study of this compound has been carried out. CETFS can form *anti* and *gauche* conformers due to restricted

☆ Dedicated to Professor Marit Trætteberg on the occasion of her 70th birthday.

* Corresponding author. Tel.: +47-22-85-5678; fax: +47-22-85-5441.

E-mail address: peter.klaboe@kjemi.uio.no (P. Klaeboe).

[1] Permanent address: Analytical Research and Development Department, ICD Division, Bayer Corporation, Bushy Park Plant, Charleston, SC 29411, USA.

0022-2860/01/$ - see front matter
PII: S0022-2860(01)00545-2

rotation around the central C–C bond as is apparent from Fig. 1. Although CETF is named a silane, the SiF_3 group forms a substituent in an ethane. This molecule is therefore different from silanes in which the conformers are due to rotations around a Si–C or a Si–Si bond. A series of molecules containing a central C–Si linkage, including ethylchlorosilane [1], ethyl dichlorosilane [2], ethyldifluorosilane [3], chloromethyl dimethyl chlorosilane [4], bromomethyl dimethylfluorosilane [5], chloromethyl dimethyl fluorosilane [6], dichloromethyl methyl difluorosilane [7], bromomethyl dimethyl silane [8], bromomethyl methyl chlorosilane [9] and chloromethyl methyl difluorosilane [10] have recently been investigated. A number of disilanes [11–14] with a Si–Si linkage and trisilanes [15–17] (Si–Si–Si) have recently been synthesized by Hassler and co-workers and the vibrational spectra reported.

These data reveal that the potential functions in ethanes with a central C–C bond are different from those of the silanes with either a Si–C or a Si–Si bond. In the latter silanes there are lower barriers and the vibrational spectrum of the *anti* conformer is more similar to that of the *gauche* conformer than is the case in ethanes. The present spectra reveal large differences between the conformers of CETFS. Preliminary data for this compound have already been presented [18], but a full account of our results for this compound will be given in the present paper.

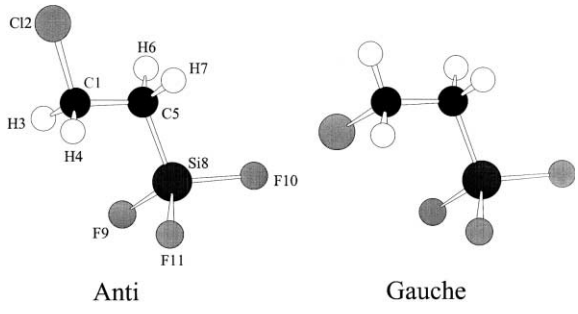

Fig. 1. The *anti* and *gauche* conformers of CETFS including numbering of the atoms for the definition of the valence coordinates.

2. Experimental

2.1. Sample preparation

The compound was prepared by the reaction of freshly sublimed antimony trifluoride with 2-chloroethyl trichlorosilane at room temperature without solvent for 1 h. Subsequently, the product was purified in a low temperature, low pressure fractionation column and the purity was checked by mass spectrometry.

2.2. Raman measurements

Raman spectra were recorded with a triple monochromator spectrometer from Dilor (model TR 30). The spectra were excited by an argon ion laser from Spectra-Physics (model 2000) using the 514.5 nm line for excitation with 90 and 180° excitation geometry. The sample was enclosed in a sealed capillary of 2 mm inner diameter and low temperature measurements of the liquid and the crystal were carried out in a Dewar cooled with nitrogen gas [19]. Additional Raman spectra of the amorphous and annealed crystalline phases of the sample deposited on a copper finger and cooled with liquid nitrogen, were measured.

Raman spectra of the liquid in two directions of polarization were recorded at room temperature. Additional spectra were obtained at 7 different temperatures between 293 and 183 K. From these spectra the enthalpy difference ΔH between the conformers were calculated in the liquid. The compound crystallized spontaneously at ca. 170 K after a moderate supercooling and Raman spectra of the crystal were recorded at 183 K. Moreover, CETFS was condensed on a copper finger at 78 K forming an amorphous solid, and after slight annealing to 120 K an intermediate phase appeared with much sharper bands. This solid converted readily to a crystalline solid containing only one conformer when the sample was annealed to 180 K. A large number of bands disappeared (Table 1) and the spectra were similar to those obtained by crystallization of the liquid.

2.3. Infrared measurements

The infrared spectra were recorded on a number of Fourier transform spectrometers in the middle infrared region (MIR): Bruker spectrometers IFS-66 and 88 (4000–450 cm^{-1}), a Nicolet model 800

Table 1
Infrared and raman spectral data for 2-chloroethyl trifluorosilane (CETFS) anti, gauche

Infrared							Raman			Interpretation	
Vapour		Ar matrix	N_2matrix	Xe-solution	Solid		Liquid	Amorphous	Crystal	*anti*	*gauche*
		5 K[b]	5 K[b]	200 K[b]	Annealed 125 K[a] 80 K[b]	Crystal 160 K[a] 80 K[b]		80 K[b]	160 K[a] 80 K[b]		
			3100 vw								
3047 vw[c]											
3006 vw		3009 vw		2997 vw			3014 m	3020 m,br	3026 m 3022 m	ν_{17}	ν_{17}
		2988 w	2989 w	2988 w			3008 m	3008 w			
2980 w 2977 m 2975 w		2982 w	2981 m		2986 m	2987 s 2981 s	2975 s,P	2982 m 2980 m	2986 w 2981 m	ν_1	ν_1
2971 w,sh		2974 m		2968 w	2957 m	2966 s 2960 s	2948 m,D	2963 m	2966 s 2961 s	ν_{18}	ν_{18}
2948 w								2949 w			
2929 w 2925 w 2921 w	A	2923 vw 2913 vvw	2933 w 2928 w	2915 w	2918 m	2929 m 2920 m	2918 s,P	2927 m	2932 s 2923 s	ν_2	ν_2
2912 vw											
2907 vw											
2903 w		2893 vw	2897 vw		2891 vw	2892 m 2888 m	2907 m,P	2886 vw	2888 w		
2900 vw		2887 vw	2888 vw				2886 vw				
2891 vw											
2772 vw			2880 vvw			2751 vw					
1469 w 1465 w, Q 1461 w	A	1460 vw↓	1461 vw↓	1458 w	1459 w 1456 m	1459 m 1454 m	1459 m,P	1459 s	1460 s		ν_3
1460 w		1456 w	1455 w↑	1453 w	1450 m	*	1452 w		*	ν_3	
1430 vw 1426 w, Q 1423 vw	A	1425 w	1425 m	1418 m	1418 m	*	1425 w	1413 w	*	ν_4	
		1423 w	1423 w		1410 vw	1411 w 1409 w					
1402 vw 1400 w, Q 1397 vw		1396 m	1397 m	1394 m	1396 s	1396 s	1398 m,P	1401 w	1399 m		ν_4
					1332 vw	1340 w	1343 vw		1336 vw		
1317 m 1313 m, Q 1309 m	A	1311 s↓	1315 m↓ 1312 m↑	1309 s	1318 s	*	1316 m,P	1312 w	*	ν_5	
1305 w		1302 w↑	1304 m↓	1299 s	1308 w	1310 w	1303 m,P	1300 m	1297 w		ν_5
1298 w		1294 m↑ 1291 m↓	1293 m	1289 m	1298 s 1289 s	1300 s 1297 s 1289 vs	1284 vw	1283 w	1296 w		ν_{19}
		1278 vw	1280 w	1276 vw	1282 w	*	1280 w,D	1276 w	*	ν_{19}	
1203 m 1199 m 1197 m		1197 s 1195 s↑ 1190 s	1200 s↑	1194 s	1198 s	*	1204 m,P	1202 w	*	ν_6	
1180 w 1176 w, Q 1172 w	A	1178 m 1174 m↓	1187 m 1183 m↓	1173 s	1179 vs	1179 vs 1177 vs	1179 m,D?	1175 m	1176 m		ν_6
1128 w		1124 m↑	1131 m↑	1123 m	1131 s	*	1127 w,D	1128 vw	*	ν_{20}	
1123 w 1119 w		1120 vw↓	1124 m↓	1120 w	1122 m 1118 m	1123 m 1121 m	1121 w,P	1118 m	1122 m		ν_{20}
1057 vw			1053 vw		1044 vw	1042 vw					
		1034 w									

Table 1 (*continued*)

Infrared						Raman			Interpretation	
Vapour	Ar matrix	N_2matrix	Xe-solution	Solid		Liquid	Amorphous	Crystal	*anti*	*gauche*
				Annealed	Crystal			160 K[a]		
	5 K[b]	5 K[b]	200 K[b]	125 K[a] 80 K[b]	160 K[a] 80 K[b]		80 K[b]	80 K[b]		
1035 s,Q	1030 s 1023 s	1026 vs↓ 1022 vs↓	1022 s	1026 s	*	1026 m,P		*	ν_7	
1030 s 1025 s 1020 s	1020 s↑	1013 m↑ 1004 m 1005 m	1004 m	1009 m 1006 s	1009 m 1006 s	1004 w,P?	1002 m	1006 s		ν_7
981 vs	1014 w 1006 s 996 w↑	971 vs↓	975 vs	954 vs 944 vs	954 vs 944 vs	963 m,br	950 w	953 w	ν_{21}	ν_{21}
972 s	976 vs	964 s↑ 955 m↑	967 s	937 vs 928 s	*		935 w	940 vw	ν_8	ν_8
	967 s 960 s↑ 951 m↑	947 w								
937 vw 934 vw 930 vw A					928 s	927 vvw	925 w	928 m		
921 w 916 w, Q 913 w A	918 m↓ 913 w	918 m↓	915 m	916 s 913 s 909 s	918 s 913 s 909 s	921 w,br,P	913 w	916 w 909 w		ν_{22}
894 s 891 s 885 vs, Q	890 vs 883 w	894 s↑ 891 s↓ 887 s	886 s	887 vs	*	884 w,P?	882 w	*	ν_{22}	
879 vs	876 s↑	877 s↓	875 s	876 s	*	875 s,P			ν_9	
874 s	871 m↓ 865 m	876 s↓	865 m	870 s	870 vs 862 m		868 m	871 m		ν_9
783 m 779 m, Q 775 m A	775 m↓ 773 m	775 m↓ 770 w↑	775 m	776 m	777 m	774 m,D	774 w	774 m		ν_{23}
745 m	749 w↑ 747 m↑ 745 w↑	743 w 740 m↓	743 m	732 m	*	739 vs,P	739 s	*	ν_{10}	
				726 vw	726 vw					
706 w 703 m, Q 699 w A	703 m↑ 698 m 695 m↑	698 m↓	699 m 695 m	699 m 690 m	* *	699 w,P	687 w	*	ν_{11},ν_{23}	
	671 w	670 m↑	670 m	669 w	671 w	671 s,P	667 s	670 s		ν_{10}
652 w 647 w 643 w	649 w 647 m↓ 645 w	645 m,br↓	645 m	638 m	639 m	643 vs,P	642 vs	640 vs		ν_{11}
				634 w	635 w	630 vw,sh 522 vw	629 vw	629 vvw		
458 w 454 w, Q 449 w	457 m↓ 455 m	456 m↓	453 m	454 m 452 m	452 s	456 w,P	460 w	452 m		ν_{12}
430 s, R 426 s, Q 422 s, P A 420 w 388 vw	423 s 422 s	424 s 423 s	422 vs	425 s 417 s	* *	424 s,P	423 m	*	ν_{12}	
366 m 362 m				363 s	366 s 363 s 359 m	365 s,P	365 m	365 m		ν_{13}
358 m				353 m 339 m	* *	352 vw,sh	354 vw,sh	*	ν_{13}	

Table 1 (*continued*)

Infrared						Raman			Interpretation	
Vapour	Ar matrix	N_2matrix	Xe-solution	Solid		Liquid	Amorphous	Crystal	*anti*	*gauche*
				Annealed 125 K[a] 80 K[b]	Crystal 160 K[a] 80 K[b]			160 K[a] 80 K[b]		
333 m 324 m				333 m 330 m	331 w	333 vw,D	332 vw	338 vw 328 vw	ν_{24}	ν_{24}
321 w 315 w, Q 310 w				320 m	315 m	323 w,P	320 w	316 m		ν_{14}
				267 m	*	265 vw,sh	265 vw,sh	*	ν_{14}	
264 w 261 m 257 m				263 m	264 m	254 w,P	260 w	257 w		ν_{15}
				246 vw	*				ν_{15}	
237 w 234 w 232 w				237 w	*	236 vs,P	237 s	*	ν_{25}	
194 w, R 189 w, Q 184 w, P	A			204 m	202 m	194 s,P	198 w	200 w		ν_{24}
143 w 138 w				179 m	179 m	160 w,br		177 w		ν_{16}
					148 w,br		*			
				112 w	117 w	110 vw	106 w,sh	* 96 w	ν_{16} lattice	
97 m					79 m	88 w,br		81 w	ν_{26}	ν_{26}
83 m 78 m 71 m							76 m	77 m	ν_{27}	ν_{27}
							65 m	66 m	lattice	
							50 w	47 m	lattice	
							41 w	29 m	lattice	
							26 m	20 m	lattice	

[a] Annealing temperature.
[b] Recording temperature.
[c] Abbreviations: s, strong; m, medium; w, weak; v, very; sh, shoulder; br, broad; P, polarized; D, depolarised. A, B and C denote vapour contours; P, Q, and R rotational transitions; asterisks denote bands vanishing in the crystal spectra; arrows pointing upwards and downwards signify matrix bands which increase and decrease in intensities after annealing.

(4000–450 cm^{-1}) and a Perkin–Elmer model 2000 (4000–450 cm^{-1}) spectrometer were employed. Two vacuum spectrometers, one from Bruker (model IFS-113v) and one from Bomem, model DA 3.002 were used in the far infrared region (FIR) (600–50 cm^{-1}). Except for the latter which had a helium cooled silicon bolometer, all the spectrometers had DTGS detectors. Beamsplitters of Ge substrate on KBr were employed in the MIR region, and beamsplitters with 3.5, 6.25 and 12 μ thickness of Mylar and a metal mesh beam splitter were used in the FIR region.

The vapour was studied in cells with KBr (10 cm) and polyethylene windows (20 cm and 1 m) with 1.0, 2.0 and 0.1 cm^{-1} resolution. The vapours were deposited on a CsI window in the MIR region and on a wedge shaped window of silicon in the FIR region, both cryostats were cooled with liquid nitrogen. A solid with spectra having sharp peaks, different from those of the amorphous solid was obtained after annealing to 125 K. At higher annealing temperatures of ca. 180 K a crystal was obtained and in this spectrum a number of bands present in the liquid had vanished.

MIR spectra of the sample dissolved in liquid xenon as a function of temperature in the range 173–218 K were recorded at 1.0 cm^{-1} resolution. A

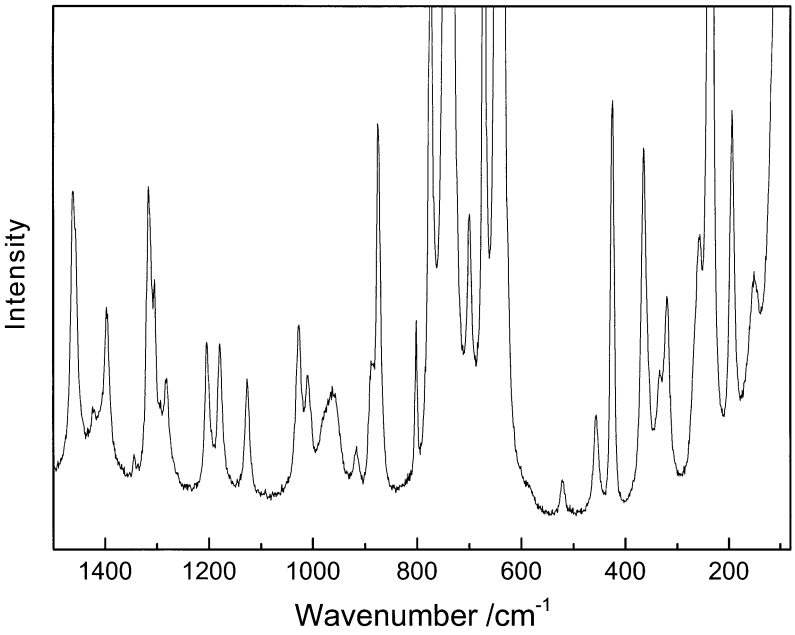

Fig. 2. Raman spectra (1500–80 cm^{-1}) of CETFS as a liquid at ambient temperature.

specially designed cryostat cell was used. It consisted of a copper block with a path length of 4 cm with wedged silicon windows sealed to the cell with indium gaskets. It was cooled by liquid nitrogen and the temperature controlled with two Pt thermoresistors. The copper cell was enclosed in an evacuated chamber having KBr windows and was connected to a vacuum line for filling and evacuation of the cell. A small amount of CETFS was condensed into the cell after it had reached the desired temperature, and the system was pressurized with xenon, which subsequently liquefied, allowing the sample to dissolve.

The sample of CETFS was diluted with argon and nitrogen (1:1000). It was deposited on a CsI window at 5 K of a Displex cryostat from APD (model HS-4) with a three stage cooling system. The MIR spectra of the unannealed matrices were first recorded at 1.0 and 0.5 cm^{-1} resolution and subsequently annealed to 15 and 20 K to observe eventual reorientations in the matrices. Further annealing to temperatures in the 25–38 K range for argon and 23–32 K for nitrogen matrices were carried out and the matrices were recooled to 5 K before recording.

3. Results

3.1. Raman spectral results

A Raman spectrum below 1500 cm^{-1} of CETFS as a liquid at ambient temperature is presented in Fig. 2, while spectra in two directions of polarization have been presented earlier [18]. Raman spectra of the annealed crystalline solid in the regions 1500–30 and 3100–2800 cm^{-1} are given in Figs. 3 and 4, respectively. Approximately 15 Raman bands present in the spectrum of the liquid disappeared after crystallization, and nearly all of these were interpreted as fundamentals. Mostly, the same bands are absent also in the corresponding infrared spectrum of the crystalline solid (see below). These vanishing bands are assigned to the second conformer, which is absent in the crystal. From a comparison between the position of the disappearing bands and the results of the normal coordinate analysis, it was concluded with certainty that the conformer present in the crystal is *gauche*.

The large number of disappearing bands reveal that the *anti* and *gauche* conformers have ca. 18

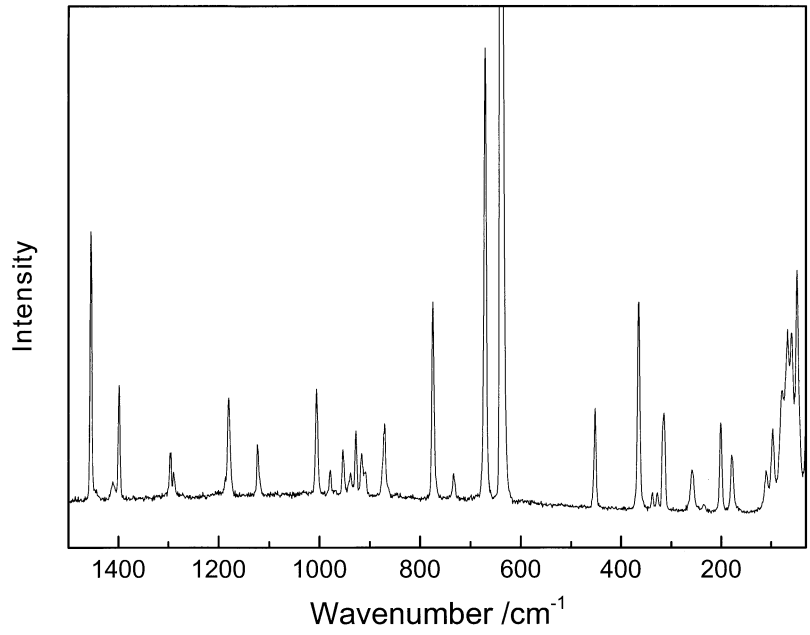

Fig. 3. Raman spectra (1500–30 cm^{-1}) of CETFS as a crystal annealed to 160 K, recorded at ca. 80 K.

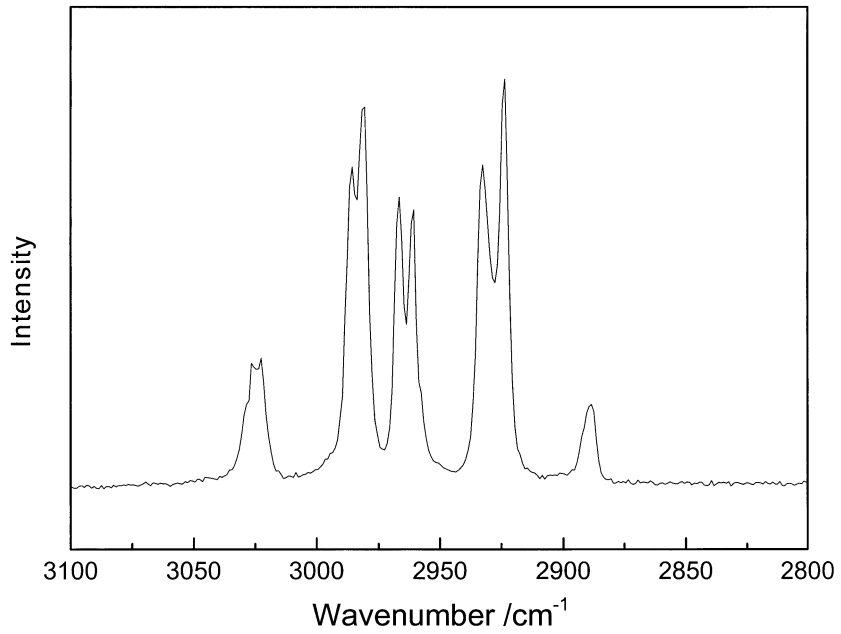

Fig. 4. Raman spectra (3100–2800 cm^{-1}) of CETFS as a crystal annealed to 160 K, recorded at ca. 80 K.

fundamentals which appear at separate wave numbers, whereas 9 of the vibrational modes of one conformer overlap those of the other. In silanes with a central C–Si bond [1–10] it is generally observed that only a few band pairs of different conformer are present. This is also the case in silanes with a Si–Si central bond [11–17].

Raman spectra of the liquid were recorded at 8 temperatures between 293 and 183 K. Small intensity variations with temperature of certain bands relative to neighbouring bands were observed. They were interpreted as a displacement of the conformational equilibrium. The Raman bands which vanished upon crystallization belong to one conformer, and they were paired with other bands (often neighbours) which remained in the crystal. However, it is a priori quite uncertain if the corresponding liquid bands are characteristic of only one conformer or if they belong to overlapping bands of both conformers. In some cases the results of the force constant calculations strongly suggest that they may originate from one conformer only.

In order to determine the enthalpy difference from the variable temperature spectra, the bands of the different conformers should both have reasonably high intensities. Moreover, they should be situated on a flat background and not overlap other bands in the spectra. More important, they must be 'pure', meaning that their intensities should be due to one conformer only, with no contribution, neither from fundamentals nor from combination bands of the other conformer. Considerable discrepancies might occur between the $\Delta_{conf}H$ values obtained from different band pairs, indicating either poor signal to noise ratio, overlapping bands or an ill-defined background. Eventually, one or both bands of the pair may be contaminated with the other conformer, meaning a superposition between a fundamental of one conformer and a fundamental, combination band or overtone belonging to the other conformer.

The intensities of each band pair were fitted to the van't Hoff equation: $\ln\{I_{anti}(T)/I_{gauche}(T)\} = -\Delta_{conf}H/RT + \text{constant}$; where I_{anti}/I_{gauche} is the ratio in peak heights or integrated areas and it is assumed that $\Delta_{conf}H$ is constant with temperature. Both peak heights and integrated band areas were attempted for determining band intensities. However, in spite of careful curve resolution and determination of band areas, the calculations based upon band areas invariably showed a larger scatter than when peak heights were employed.

The following five pairs of bands were treated in the van't Hoff plots (Fig. 8 in Ref. [18]): 236/194, 236/254, 424/364, 739/669 and 1204/1179 cm^{-1} (liquid), in which the bands in the nominator vanished in the crystal (*anti* conformer). They gave the values: 1.0, 0.6, 0.5, 1.0 and 0.8, respectively, averaging $\Delta H(anti - gauche) = 0.8 \pm 0.3$ kJ mol^{-1}.

Low temperature Raman spectra of CETFS were independently recorded when the sample was deposited on a cold copper finger, cooled by liquid nitrogen. The amorphous solid first formed at 78 K mostly contained the same bands as in the liquid, but had broader features. When a thin layer was deposited comparable to the infrared cryostat, an apparent intermediate phase was obtained after annealing to ca. 130 K and recooled to 78 K. It appeared crystalline from visual observation, the bands were shifted and they were sharper than those of the amorphous phase. However, no bands vanished in this phase and both conformers were undoubtedly present. After annealing to ca. 160 K a real crystal was formed. The Raman spectrum appeared to be the same as that obtained by cooling the liquid until crystallization and was presented in Figs. 3 and 4, meaning that it only contained one conformer (*gauche*). A thick deposit of CETFS readily turned into a real crystal during deposition requiring negligible annealing.

3.2. Infrared spectral results.

An infrared survey spectrum of CETFS as a vapour in the range 1500–400 cm^{-1} at 8 Torr pressure in a 10 cm cell with resolution 1 cm^{-1} is presented in Fig. 5. A vapour spectrum in FIR (600–50 cm^{-1}) has previously been given in Ref. [18]. An additional FIR spectrum (350–30 cm^{-1}) recorded in a folded cell with 1 m path at 0.1 cm^{-1} resolution, using a He-cooled bolometer as detector, is given in Fig. 6. A number of well resolved vapour contours were observed in the spectra, some of them like 2925, 1465, 1426, 1313, 1176, 934, 916, 779, 703, 426 and 189 cm^{-1} had apparent A-type contours with a PR separation of ca. 8 cm^{-1}. In other cases the possible rotational contours may be a superposition of vapour bands from the two conformers.

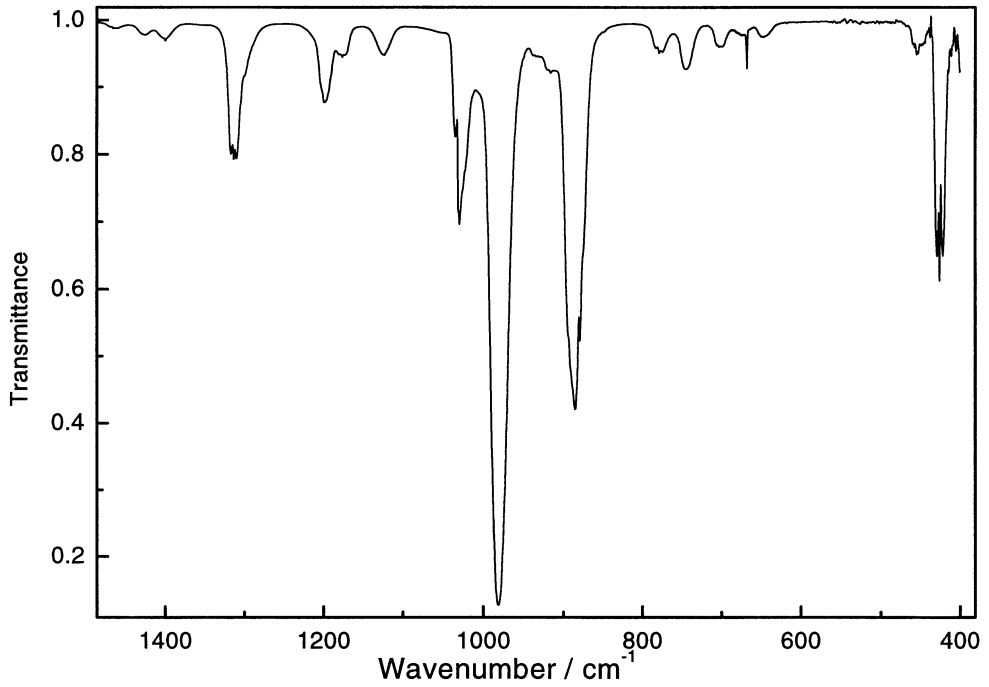

Fig. 5. A middle infrared (MIR) spectrum (1500–400 cm^{-1}) of CETFS as a vapour, 10 cm path, 8 Torr, 1 cm^{-1} resolution.

MIR spectra of the amorphous and crystalline solids recorded in a restricted range (850–600 cm^{-1}) at 80 K are found in Fig. 7 whereas corresponding FIR spectra (650–100 cm^{-1}) were presented in Ref. [18]. Three curves are given in these spectra, one presenting an unannealed solid (solid line), one a solid annealed to 125 K, dashed line and finally a crystal annealed to 160 K (dotted line), all recorded at 80 K. As is apparent from these figures, when the sample was annealed to ca. 125 K and recooled to 80 K, the IR bands were all much sharper. They were shifted from those of the amorphous solid formed at 80 K, which had very broad features. The infrared bands present in the amorphous solid and in the phase obtained at 125 K, but vanishing in the spectra of stable crystal, are the same as those disappearing in the Raman spectra (see above).

The existence of two crystals, each containing a different conformer, has recently been observed in three silanes: dichloromethyl methyl difluorosilane [7], bromomethyl dimethyl silane [8] and chloromethyl methyl difluorosilane [10]. In CETFS the situation was different since the 125 K phase contained both conformers while the crystal formed at 160 K crystal contained only a single rotamer (*gauche*).

In order to obtain information on the value of the enthalpy difference between the two conformers in an inert solvent a variable temperature study in liquified xenon was carried out. The sample was dissolved in liquefied xenon and the spectra were recorded at difference temperatures from −55 to −100°C (223–173 K). A MIR survey spectrum in xenon is presented in Fig. 8. Low interactions are expected to occur between the dissolved sample and the surrounding xenon atoms and, consequently, only small frequency shifts are anticipated when passing from the gas phase to the liquid noble gas solution [20–24]. A significant advantage of this type of temperature study is that the conformer bands are better resolved in comparison with those in the infrared spectrum of the gas. However, in this particular molecule there are shifts calculated as high as 84 cm^{-1} (ν_{23}) between the *anti* and *gauche* conformers (see below). As is apparent from the data in Table 1 there are several conformer bands in Xe-solution which are well separated.

The best separated conformer bands in xenon solution are those assigned to the C–Cl stretch, CH_2 rock

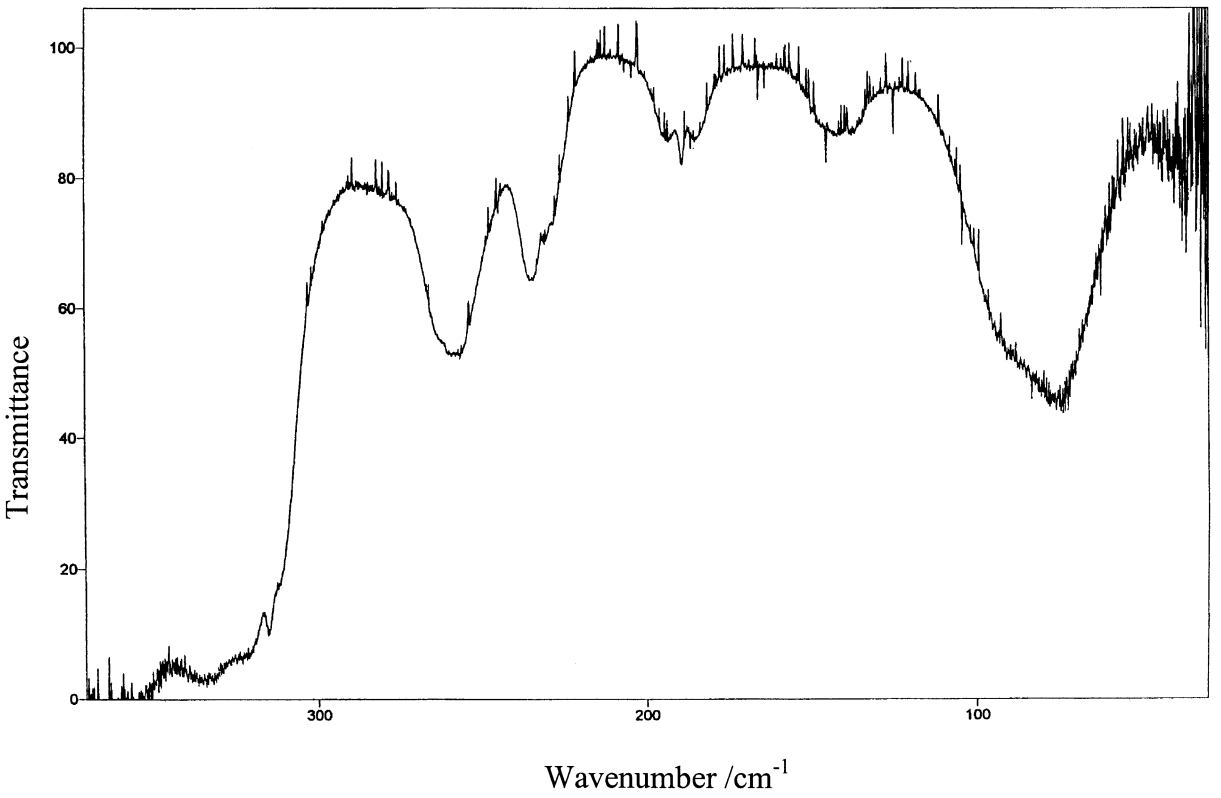

Fig. 6. A far infrared (FIR) spectrum (350–40 cm^{-1}) of CETFS as a vapour, 1 m path, pressure 33 Torr, 0.1 cm^{-1} resolution.

and Si–C stretching modes. Additionally, they are well suited for variable temperature measurements with the exception of the band at 645 cm^{-1}. The relative intensity of the above mentioned fundamentals of the *anti* and *gauche* conformers were measured as a function of temperature and their ratios were determined. The two overlapping bands at 699 and 695 cm^{-1} both belong to the *anti* conformer (ν_{23} and ν_{11}, respectively) and their measured intensities are combined together and used with other fundamentals of the *gauche* conformer to calculate intensity ratios. The two *anti* bands at 743 and 699 cm^{-1} and the *gauche* bands at 775 and 670 cm^{-1} were combined to give four band pairs, and these data are collected in Table 2. Ten sets of spectral data points covering 5 degrees intervals from 173 to 218 K were obtained for these band pairs (Fig. 9). Applying the van't Hoff equation (see above) the values in Table 2 were obtained, giving an average value $\Delta H(gauche - anti) = 0.66 \pm 0.13$ kJ mol^{-1}. Two plots are presented in Fig. 10, the *anti* band is present in the nominator, the *gauche* band in the denominator. Thus, the *anti* conformer is more stable in liquid xenon and probably in the vapour while *gauche* is more stable in the liquid, and remains in the crystal (see below).

Additional infrared spectra of CETFS were recorded in argon (Fig. 11) and nitrogen matrices (Fig. 12) in mixing ratios 1:500 and 1:1000, deposited at 4.8 K. These spectra were recorded with different times of deposition in order to cover the extremely intense Si–F_3 stretching bands 1000–850 cm^{-1} and the weaker absorption in the remaining regions. Supposedly, the conformational equilibrium of the vapour phase is maintained when the gas mixture is quickly frozen on the CsI window at 4.8 K, provided that the barrier to conformational equilibrium is above 3.5 kJ mol^{-1} [20]. Smaller spectral changes occur after annealing around 20 K. They are often different in argon and nitrogen matrices and are interpreted as site effects due to relaxation of CETFS in the matrix

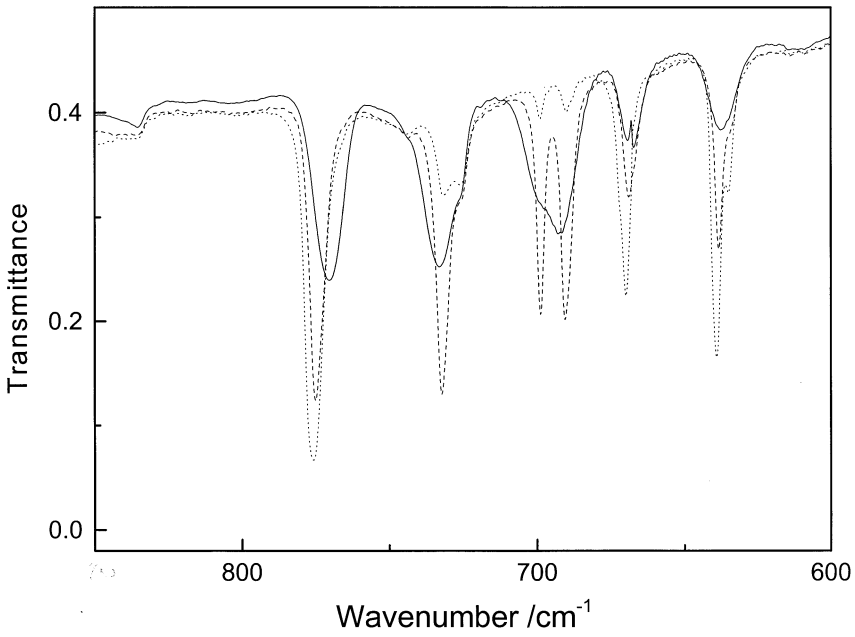

Fig. 7. MIR spectra (850–600 cm^{-1}) of CETFS at 80 K, unannealed (solid line), annealed to 125 K (dashed) and to 160 K (dotted).

cages. At higher annealing temperatures (22–38 K) changes were observed both in the argon and nitrogen matrix spectra which were correlated with conformational changes.

Relatively small intensity changes occurred in these spectra after annealing. With a few exception, the bands having increased intensities in the matrix spectra after annealing, are the same as those which are enhanced in xenon solutions at lower temperatures and disappear on crystallization. Consequently, both the argon and nitrogen matrices stabilize a conformer, which disappears in the crystal and which is also the

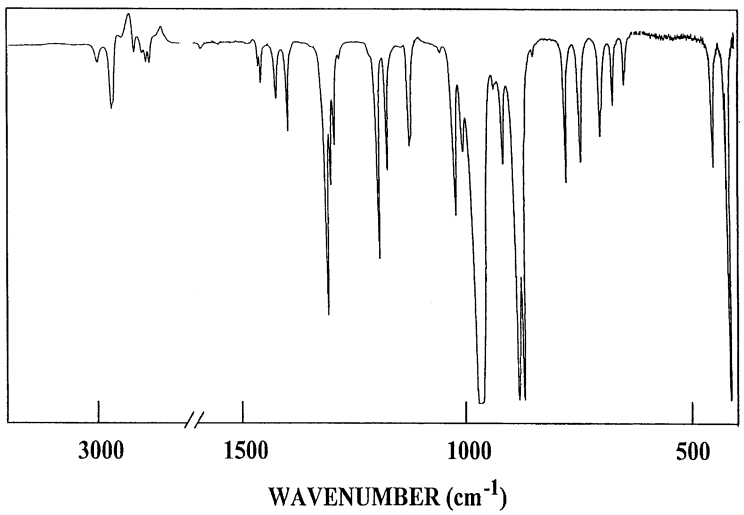

Fig. 8. A MIR spectrum of CETFS dissolved in liquid xenon at 223 K.

Table 2
Temperature and intensity ratios for the conformational study of 2-chlorotrifluorosilane (CETFS) in liquid xenon

T (°C)	1000/T (K)	I_{743}/I_{775}	−lnk	I_{699}/I_{670}	−lnk	I_{699}/I_{775}	−lnk	I_{743}/I_{670}	−lnk
−55	4.587	1.175	−0.1612	2.569	−0.9436	0.9341	0.0682	3.2316	−1.1730
−60	4.695	1.193	−0.1766	2.501	0.9166	0.9646	0.0360	3.0931	−1.1292
−65	4.808	1.177	−0.1625	2.527	−0.9272	0.8159	0.2035	3.0978	−1.1307
−70	4.926	1.198	−0.1803	2.625	−0.9649	0.9832	0.0169	3.1971	−1.1622
−75	5.051	1.189	−0.1727	2.621	−0.9636	0.9697	0.0308	3.2125	−1.1671
−80	5.181	1.200	−0.1822	2.681	−0.9860	1.0043	−0.0043	3.2023	−1.1639
−85	5.319	1.212	−0.1921	2.768	−1.0182	1.0273	−0.0269	3.2658	−1.1835
−90	5.464	1.198	−0.1807	2.627	−0.9657	1.0270	0.0266	3.0639	−1.1197
−95	5.618	1.223	−0.2016	2.726	−1.0027	1.0410	−0.0402	3.3030	−1.1948
−100	5.780	1.222	−0.2006	2.956	−1.0839	0.0711	0.0687	3.3725	1.2157
ΔH^a			21 ± 4		72 ± 16		99 ± 31		28 ± 16

[a] Average $\Delta H = 0.66 \pm 0.13$ kJ mol^{-1} with the *anti* conformer the more stable form.

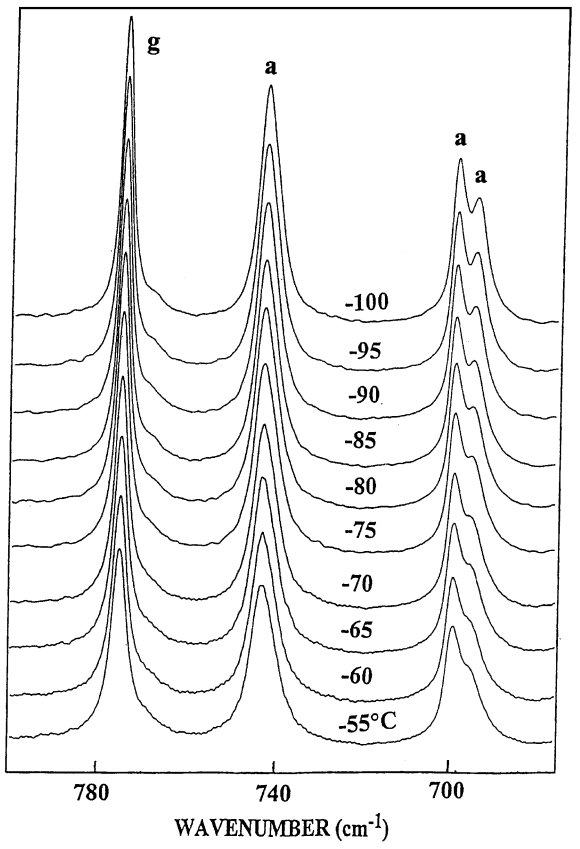

Fig. 9. MIR spectra (800–670 cm^{-1}) of CETFS in liquid xenon at 10 temperatures between 223 and 173 K.

high energy conformer in the liquid. Hence, the high energy conformer in the liquid is the low energy conformer in liquid xenon and in the argon and nitrogen matrices. To be discussed below, the conformer present in the stable crystal, which is also the low energy conformer in the liquid but the high energy in the matrices is definitely shown to be *gauche*.

The lowest annealing temperature at which the equilibrium of the solute molecule was displaced

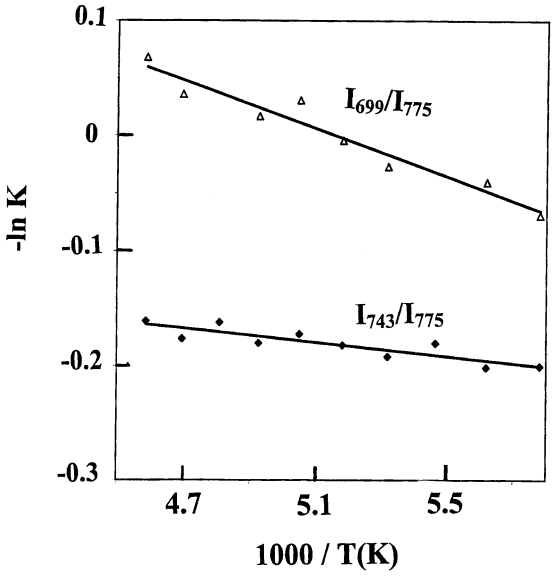

Fig. 10. Van't Hoff plots of the band pairs 699/775 and 743/775 cm^{-1} of CETFS dissolved in liquid xenon.

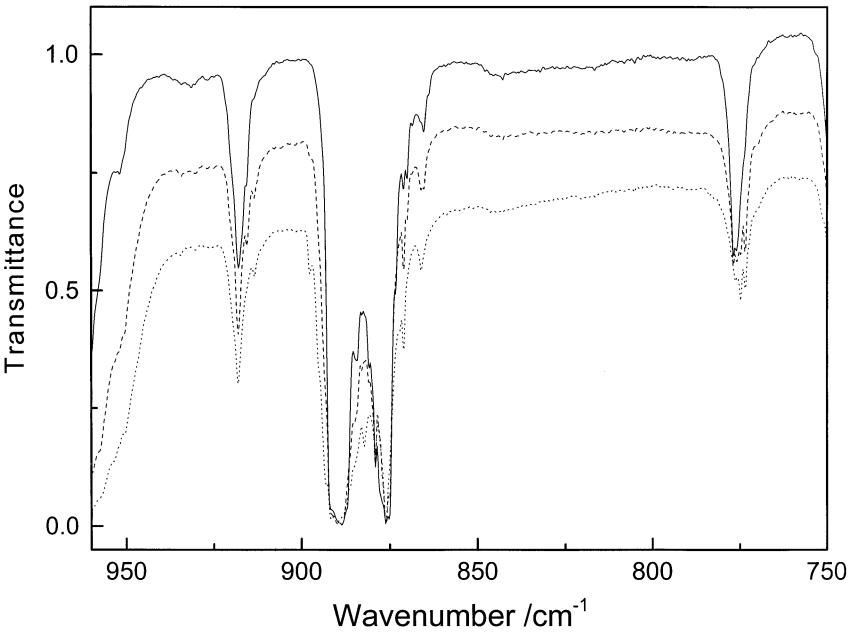

Fig. 11. MIR spectra (960–750 cm^{-1}) of CETFS in an argon matrix (1:1000) at 4.8 K, unannealed (solid line), annealed to 33 K (dashed line) and to 38 K (dotted line).

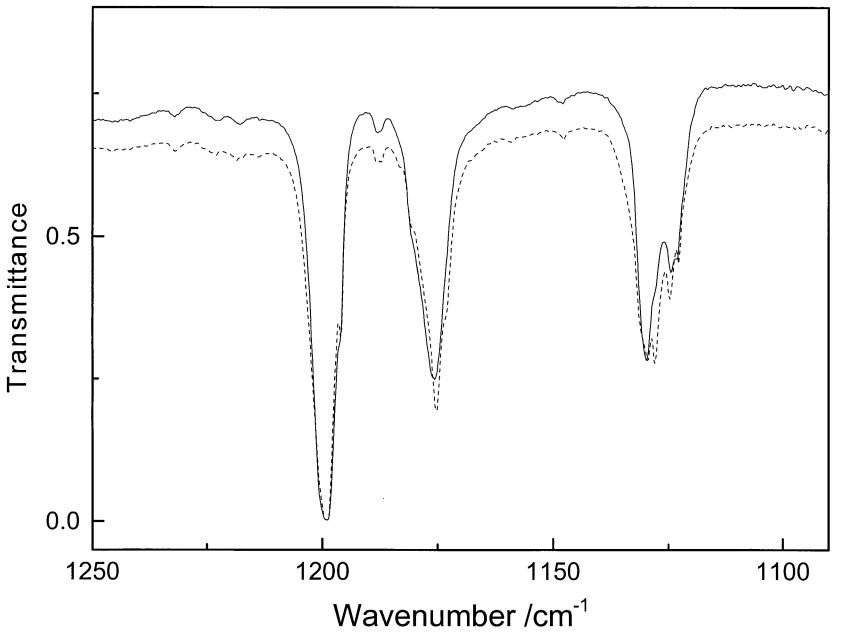

Fig. 12. MIR spectra (1250–1090 cm^{-1}) of CETFS in nitrogen matrix (1:1000) at 4.8 K, unannealed (solid line) and annealed to 31 K (dashed line).

from the high to the low energy conformation, was used for estimating the conformational barrier. For both matrices this temperature was ca. 30 K. From the curves correlating annealing temperature and activation energy/barrier height given by Barnes [25] the conformational barrier was estimated to be 6–7 kJ mol^{-1}. If secondary effects due to matrix viscosity or matrix-solute interactions are neglected this barrier height may also be valid for the isolated molecules in the vapour phase. The observed wave numbers for the infrared and Raman bands of CETFS in the various states of aggregation are listed in Table 1. The bands vanishing in the crystalline solids are equipped with asterisks. Infrared bands in argon and nitrogen matrices are fitted with arrows pointing upwards or downwards if the bands increase or decrease in intensity after annealing, respectively.

3.3. Quantum chemical calculations

Hartree Fock quantum chemical calculations were performed using the GAUSSIAN-94 programs [26]. To allow an easy comparison with the series of halomethyldimethylhalosilanes studied earlier, the basis function 6-311G* was employed in the RHF approximation, while calculations of the wave numbers were also performed with MP2/G-31G (d). The minima on the potential surface were found by relaxing the geometry. Bond distances and angles for both the *anti* and *gauche* conformers of CETFS were listed, but have not been presented for the sake of brevity.

The conformational energy difference was calculated to be 3.8 kJ mol^{-1} with *anti* being the low energy conformer.

3.4. Normal coordinate calculations

Analytical H–F force constants were derived for each of the two conformers of CETFS using the 6-311G* basis set. The calculated ab initio force constants were transformed from Cartesian to symmetry coordinates, derived from a set of valence coordinates. The ab initio calculated wave numbers are invariably larger than the experimental values. In order to make a complete assignment of the observed infrared and Raman bands, a normal coordinate analysis with scaled force constants was carried out. Scaling factors of 0.9 for the stretching and bending modes above, and no scaling for the modes below 400 cm^{-1} were employed for easy comparison with the earlier silanes [4–10]. The infrared intensities, Raman scattering cross sections and Raman polarization ratios were calculated and these data are also listed in Tables 3 and 4. The calculated wavenumbers for the *anti* and *gauche* conformers reveal that in 16 cases the shifts were larger than 10 cm^{-1}, while for ν_{10}, ν_{14}, ν_{16} and ν_{23} the shifts were larger than 50 cm^{-1}. This is in contrast to the silanes with C–Si bond were the two rotamers had much smaller spectral differences.

The PED (potential energy distribution) are expressed in terms of the symmetry coordinates. The normalised symmetry coordinates have been constructed from a set of valence coordinates which are given in Table 5 while the numbering of the atoms appear in Fig. 1. Only PED terms larger than 10% have been included in Tables 3 and 4 and the largest term in PED is also described in terms of valence coordinates in these tables. The C–H, C–Cl and the Si–F stretching modes are reasonably well localized, but the CH_3 rock, C–C stretches and the skeletal deformations are highly mixed. Obviously, the vibrational modes for the *anti* conformer, separated into symmetry species A′ and A″ are more localized than those of the *gauche* conformer in which all the modes belong to the same species.

4. Discussion

4.1. Phase transitions

As is apparent from Fig. 7 the IR spectra of the low temperature solid deposits on the CsI or Si window at 80 K change considerably upon annealing. Similar features were observed on the copper finger of the Raman cryostat, but the effect was not as pronounced. The unannealed substance looked glassy and gave spectra quite similar to those of the liquid. After annealing to ca. 125 K the compound changed appearance to a ‘frosty look’. The IR bands become much sharper and they are in nearly every case shifted a few wavenumbers (8–1 cm^{-1}) from the position of the amorphous phase. Frequently they are split into more components as apparent for ν_7, ν_8, ν_{11}, ν_{12}, ν_{13}, ν_{19}, ν_{20} and ν_{21}. When the samples were annealed

Table 3
Observed and calculated fundamental modes of the *anti* conformer in CETFS

		Observed[a]	I_{IR}	I_R	Calculated[b]	Scaled[c]	I_{IR}[d]	I_R[e]	ρ[f]	PED[g]	Description
A′	ν_1	2977	w	m	3271	2944	22.2	74.4	0.09	$99S_1$	Sym CH_2 stretch in–CH_2Cl
	ν_2	2925	w	s,P	3198	2878	4.3	88.4	0.12	$99S_2$	Sym CH_2 stretch in –CH_2–
	ν_3	1460	w	w	1631	1468	1.1	6.3	0.67	$94S_8$	CH_2 scissor in –CH_2Cl
	ν_4	1426	w	w	1588	1429	6.8	4.3	0.70	$94S_{12}$	CH_2 scissor in –CH_2–
	ν_5	1313	s	w	1487	1339	93.0	2.0	0.58	$70S_9 + 16S_{13}$	CH_2 wag in –CH_2Cl
	ν_6	1199	s	w,P	1354	1218	27.7	1.1	0.26	$67S_{13} + 23S_9$	CH_2 wag in –CH_2–
	ν_7	1035	m	m,P	1102	992	37.1	5.9	0.52	$82S_6$	C–C stretch
	ν_8	937	vw	w	1036	932	223.8	0.9	0.52	$90S_4$	Antisym SiF_3 stretch
	ν_9	874	m	m	943	849	234.2	0.1	0.45	$64S_3 + 21S_7$	Sym SiF_3 stretch
	ν_{10}	745	m	vs,P	802	721	38.4	27.4	0.27	$45S_5 + 19S_{10} + 15S_{11}$	C–Cl stretch
	ν_{11}	703	m	w,P	738	664	10.5	1.8	0.31	$41S_7 + 24S_3 + 23S_5$	C–Si stretch
	ν_{12}	426	s	m,P	448	403	136.4	0.9	0.16	$61S_{14} + 10S_{11}$	Sym $CSiF_3$ deformation
	ν_{13}	358	m	vw	372	372	23.4	0.8	0.46	$45S_{15} + 17S_{10} + 12S_{16}$	Antisym $CSiF_3$ deformation
	ν_{14}	267[h]	m	vw	275	275	6.4	0.1	0.72	$30S_{15} + 24S_{10} + 23S_{16}$	$CSiF_3$ wag
	ν_{15}	246[h]	vw	–	243	243	3.0	3.2	0.38	$30S_{10} + 15S_7 + 13S_8 + 14S_{14}$	CCCl bend
	ν_{16}	112[h]	w	vw	103	103	6.0	0.7	0.74	$46S_{11} + 26S_{12} + 20S_{16}$	CCSi bend
A″	ν_{17}	3006	vw	m	3331	2997	9.2	42.1	0.75	$98S_{17}$	Antisym CH_2 stretch in CH_2Cl
	ν_{18}	2971	w	vw	3237	2914	4.0	69.0	0.75	$98S_{18}$	Antisym CH_2 stretch in –CH_2–
	ν_{19}	1280[i]	vw	w,D	1432	1289	0.0	8.2	0.75	$58S_{21} + 33S_{23}$	CH_2 twist in CH_2Cl
	ν_{20}	1128	w	w,D	1256	1131	13.3	1.1	0.75	$45S_{21} + 42S_{23} + 10S_{20}$	CH_2 twist in –CH_2–
	ν_{21}	981	vs	vw	1048	943	197.1	0.4	0.75	$62S_{20} + 16S_{21} + 10S_{22}$	Antisym SiF_3 stretch
	ν_{22}	885	s	w,P	975	877	43.1	2.2	0.75	$42S_{20} + 29S_{19} + 22S_{23}$	CH_2 rock in CH_2Cl
	ν_{23}	703	vw,D	w,P	766	689	7.3	0.1	0.75	$58S_{22} + 23S_{20}$	CH_2 rock in –CH_2–
	ν_{24}	328	vw	–	347	347	23.5	0.3	0.75	$77S_{25} + 10S_{24}$	$CSiF_3$ twist
	ν_{25}	234	w	s,P	241	241	0.3	0.4	0.75	$67S_{24} + 12S_{25}$	$CSiF_3$ rock
	ν_{26}	97	w	w	78	78	6.9	1.5	0.75	$58S_{26} + 14S_{22}$	CH_2Cl torsion
	ν_{27}	78	m	m	52	52	0.3	0.1	0.75	$85S_{27}$	SiF_3 torsion

[a] From IR vapour spectra, except when noted.
[b] Calculated at the HF/6-311G* level.
[c] Wavenumbers above 400 cm^{-1} have been scaled by 0.9; A′ and A″ denote symmetry species.
[d] Calculated infrared intensities (km mol^{-1}).
[e] Calculated Raman cross sections ($Å^4$ mol^{-1}).
[f] Polarisation ratios.
[g] For definition of symmetry coordinates, see Table 5; terms below 10% are omitted.
[h] From IR amorphous phase,
[i] Raman liquid.

Table 4
Observed and calculated fundamental modes of the *gauche* conformer in CETFS

	Observed[a]	I_{IR}	I_R	Calculated[b]	Scaled[c]	I_{IR} [d]	I_R [e]	ρ [f]	PED[g]	Description
ν_1	3006	vw	m	3335	3002	9.5	61.0	0.73	$99S_{17}$	Antisym CH_2 stretch in CH_2Cl
ν_2	2977	vw	s,P	3277	2949	28.1	95.1	0.07	$99S_1$	Sym CH_2 stretch in–CH_2Cl
ν_3	2971	m	w	3230	2907	3.8	80.3	0.62	$87S_{18} + 12S_2$	Antisym CH_2 stretch in $-CH_2-$
ν_4	2925	vw	vw	3180	2862	8.9	110.3	0.18	$87S_2 + 12S_{18}$	Sym CH_2 stretch in $-CH_2-$
ν_5	1465	w	m,P	1634	1471	1.1	9.4	0.71	$95S_8$	CH_2 scissor in $-CH_2Cl$
ν_6	1400	w	m,P	1574	1417	12.3	7.7	0.71	$97S_{12}$	CH_2 scissor in $-CH_2-$
$?\nu_7$	1305	w	w,D	1473	1326	49.6	1.1	0.69	$82S_9$	CH_2 wag in $-CH_2Cl$
ν_8	1298	m	vw	1458	1312	23.5	1.7	0.59	$56S_{13} + 23S_{21}$	CH_2 wag in $-CH_2-$
ν_9	1176	w	w,D	1319	1187	19.0	7.1	0.72	$26S_{21} + 26S_{23} + 20S_{13} + 12S_6$	CH_2 twist in $-CH_2-$
$\nu_{10}?$	1121	w	w,P	1250	1125	11.4	4.2	0.68	$44S_{21} + 40S_{23}$	CH_2 twist in CH_2Cl
ν_{11}	1025	m	w,P	1093	984	32.0	3.7	0.58	$56S_6 + 11S_{20}$	C–C stretch
ν_{12}	981	vs	vw	1045	940	178.1	1.8	0.74	$61S_{19} + 10S_6 + 10S_{20}$	Antisym SiF_3 stretch
ν_{13}	972	vw	vw	1033	929	225.4	1.1	0.74	$70S_4$	Antisym SiF_3 stretch
ν_{14}	916	w	w,P	1000	900	79.0	1.3	0.74	$40S_{20} + 18S_{19} + 15S_4 + 10S_{13}$	CH_2 rock in CH_2Cl
ν_{15}	879	m	m,P	930	837	216.9	0.8	0.40	$70S_3 + 13S_7$	Sym SiF_3 stretch
ν_{16}	779	m	m,P	859	773	27.2	4.0	0.41	$40S_{22} + 16S_{10} + 13S_5$	CH_2 rock in $-CH_2-$
ν_{17}	671[h]	m	m,P	716	645	17.5	7.5	0.67	$45S_5 + 16S_7 + 13S_{22}$	C–Cl stretch
ν_{18}	645	vw	vs,P	676	608	16.3	15.2	0.06	$35S_7 + 28S_5$	C–Si stretch
ν_{19}	454	w	w,D	485	436	28.0	0.6	0.74	$29S_{11} + 18S_{10} + 13S_{12} + 12S_{14}$	CCSi bend
ν_{20}	364	s	m,P	378	378	75.9	1.8	0.55	$63S_{14} + 12S_{10}$	Sym $CSiF_3$ deformation
ν_{21}	328	m	w,D	349	349	20.7	0.5	0.71	$62S_{25}$	$CSiF_3$ twist
ν_{22}	315	m	w,P	333	333	26.0	1.1	0.73	$65S_{15} + 21S_{10}$	$CSiF_3$ rock
ν_{23}	261	m	w,P	267	267	1.8	0.5	0.43	$34S_{24} + 13S_{10} + 13S_{11} + 13S_{26}$	Antisym $CSiF_3$ deformation
ν_{24}	189	w	m,P	198	198	1.6	0.6	0.68	$39S_{16} + 18S_{10} + 15S_{24}$	$CSiF_3$ wag
ν_{25}	140	w	w	154	154	1.7	0.6	0.74	$36S_{11} + 20S_{12} + 12S_{16}$	CCCl bend
ν_{26}	97	w	w	83	83	1.1	0.4	0.74	$38S_{26} + 23S_{11} + 12S_{12}$	CH_2Cl torsion
ν_{27}	78	m	m	36	36	2.4	0.6	0.74	$69S_{27}$	SiF_3 torsion

[a] From IR vapour spectra, except when noted.
[b] Calculated at the HF/6-311G* level.
[c] Wavenumbers above 400 cm^{-1} have been scaled by 0.9.
[d] Calculated infrared intensities (km mol^{-1}).
[e] Calculated Raman cross sections ($Å^4$ mol^{-1}).
[f] Polarisation ratios.
[g] For definition of symmetry coordinates, see Table 5; terms below 10% are omitted.
[h] Raman liquid.

to temperatures around 160 K or if the liquid was cooled to this temperature range a crystal was formed and several IR and Raman bands vanished in this phase. It is characteristic for the crystal that a number of bands appeared as doublets (10 instances) or even as triplets (3 instances) revealing interactions between neigbouring molecules in the same unit cell.

4.2. Conformations

It can be seen from Table 1 that in 18 cases IR and/or Raman bands present in the vapour, liquid and amorphous phase vanished in the spectra of the crystal. In the large majority of cases the disappearing bands have been interpreted as fundamental modes of the conformer vanishing in the crystal. Only a few weak band have been assigned to combination bands or overtones. These observations have made it feasible to divide the observed bands to the *anti* or *gauche* conformers. Only in relatively few cases the vibrational modes for the two rotamers overlap. Also, the bands vanishing in the crystal can be correlated with those being enhanced in the Raman spectra of the liquid at increasing temperatures. They are also the same as the IR bands being enhanced in liquid xenon at lower temperatures or IR bands of the matrix

Table 5
Internal coordinates used in describing the vibrational modes of CETFS (for numbering of valence coordinates, see Fig. 1)

	Description	Definition
A′	CH_2 sym. stretch in $-CH_2Cl$	$S_1 = (\Delta R_{1,3} + \Delta R_{1,4})/\sqrt{2}$
	CH_2 sym. stretch in $-CH_2-$	$S_2 = (\Delta R_{5,6} + \Delta R_{5,7})/\sqrt{2}$
	SiF_3 sym. stretch	$S_3 = (\Delta R_{8,10} + \Delta R_{8,9} + \Delta R_{3,8,11})/\sqrt{3}$
	SiF_3 antisym. stretch	$S_4 = (2\Delta R_{8,10} - \Delta R_{8,9} - \Delta R_{3,8,11})/\sqrt{6}$
	SiF_2 sym. stretch	$S_5 = \Delta R_{1,2}$
	C–Cl stretch	$S_6 = \Delta R_{1,5}$
	C–C stretch	$S_7 = \Delta R_{5,8}$
	CH_2 scissor in $-CH_2Cl$	$S_8 = (\Delta\alpha_{5,1,3} + \Delta\alpha_{5,1,4} + \Delta\alpha_{2,1,3} + \Delta\alpha_{2,1,4})/2$
	CH_2 wag in $-CH_2Cl$	$S_9 = (\Delta\alpha_{5,1,3} + \Delta\alpha_{5,1,4} - \Delta\alpha_{2,1,3} - \Delta\alpha_{2,1,4})/2$
	C–C–Cl bend	$S_{10} = \Delta\alpha_{2,1,5}$
	C–C–Si bend	$S_{11} = \Delta\alpha_{1,5,8}$
	CH_2 scissor in $-CH_2-$	$S_{12} = (\Delta\alpha_{1,5,6} + \Delta\alpha_{1,5,7} + \Delta\alpha_{8,5,6} + \Delta\alpha_{8,5,7})/2$
	CH_2 wag in $-CH_2-$	$S_{13} = (\Delta\alpha_{1,5,6} + \Delta\alpha_{1,5,7} - \Delta\alpha_{8,5,6} - \Delta\alpha_{8,5,7})/2$
	CF_3 sym. deformation	$S_{14} = (\Delta\alpha_{9,8,11} + \Delta\alpha_{9,8,10} + \Delta\alpha_{10,8,11} - \Delta\alpha_{5,8,10} - \Delta\alpha_{5,8,11} - \Delta\alpha_{5,8,9})/\sqrt{6}$
	CF_3 antisym. deformation	$S_{15} = (2\Delta\alpha_{9,8,11} - \Delta\alpha_{9,8,10} - \Delta\alpha_{10,8,11})/\sqrt{6}$
	CF_3 antisym. Deformation	$S_{16} = (2\Delta\alpha_{5,8,10} - \Delta\alpha_{5,8,11} - \Delta\alpha_{5,8,9})/\sqrt{6}$
A″	CH_2 antisym. stretch in $-CH_2Cl$	$S_{17} = (\Delta R_{1,3} - \Delta R_{1,4})/\sqrt{2}$
	CH_2 antisym. stretch in $-CH_2-$	$S_{18} = (\Delta R_{5,6} - \Delta R_{5,7})/\sqrt{2}$
	CF_2 antisym. stretch	$S_{19} = (\Delta R_{8,9} - \Delta R_{8,11})/\sqrt{2}$
	CH_2 rock in $-CH_2Cl$	$S_{20} = (\Delta\alpha_{5,1,3} - \Delta\alpha_{5,1,4} + \Delta\alpha_{2,1,3} - \Delta\alpha_{2,1,4})/2$
	CH_2 twist in $-CH_2Cl$	$S_{21} = (\Delta\alpha_{5,1,3} - \Delta\alpha_{5,1,4} - \Delta\alpha_{2,1,3} + \Delta\alpha_{2,1,4})/2$
	CH_2 rock in $-CH_2-$	$S_{22} = (\Delta\alpha_{1,5,6} - \Delta\alpha_{1,5,7} + \Delta\alpha_{8,5,6} - \Delta\alpha_{8,5,7})/2$
	CH_2 twist in $-CH_2-$	$S_{23} = (\Delta\alpha_{1,5,6} - \Delta\alpha_{1,5,7} - \Delta\alpha_{8,5,6} + \Delta\alpha_{8,5,7})/2$
	CF_3 twist	$S_{24} = (\Delta\alpha_{9,8,10} - \Delta\alpha_{10,8,11} + \Delta\alpha_{5,8,11} - \Delta\alpha_{5,8,9})/2$
	CF_3 rock	$S_{25} = (\Delta\alpha_{9,8,10} - \Delta\alpha_{10,8,11} - \Delta\alpha_{5,8,11} + \Delta\alpha_{5,8,9})/2$
	$-CH_2Cl$ torsion	$S_{26} = (\Delta\tau_{2,1,5,8} + \Delta\tau_{3,1,5,7} + \Delta\tau_{4,1,5,6})/\sqrt{3}$
	$-CF_3$ torsion	$S_{27} = (\Delta\tau_{1,5,8,10} + \Delta\tau_{6,5,8,11} + \Delta\tau_{7,5,8,9})/\sqrt{3}$

isolated CETFS being enhanced after annealing. Neither the Raman polarization data nor the ab initio calculated energies could answer the following question: do the bands vanishing in the spectra of the crystal belong to the *anti* or the *gauche* conformer? The calculated energies for the *anti* and *gauche* rotamers derived from the ab initio calculations have large uncertainties. However, the force constants and the wave numbers after appropriate scaling usually give a good agreement with those of the observed fundamentals. Within the group frequency regions for the CH_3, CH_2 or SiF_3 stretching and deformation vibrations, the calculated wave numbers for the *anti* and *gauche* fundamentals frequently overlap (Tables 3 and 4). The fundamentals in the *anti* conformer are numbered as ν_1–ν_{16} in species A′ and as ν_{17}–ν_{27} in A″ and the modes are listed correspondingly in the *gauche* conformer in order to maintain the similarity between the *anti* and *gauche* modes. Totally there are 16 instances in which the calculated values for the *anti* and *gauche* fundamentals are separated more than 10 cm^{-1}. This is apparent from the listed wavenumbers in Tables 3 and 4 for the modes:

ν_2, ν_4, ν_5, ν_6, ν_9, ν_{10}, ν_{11}, ν_{12}, ν_{14}, ν_{15}, ν_{16}, ν_{19}, ν_{22}, ν_{23}, ν_{25} and ν_{27}. Here we expect the observed infrared and Raman bands of the *anti* and *gauche* conformers to appear as separate modes which can be identified from the crystal spectra. In most cases, it was quite simple to assign the observed infrared and Raman bands to *anti*/*gauche* pairs in good agreement with these calculated shifts. It was a prerequisite that the 'correct' conformer was present in the crystal. The exceptions are the modes ν_1, ν_2, ν_8, ν_{17}, ν_{18}, ν_{21}, ν_{26} and ν_{27} were the rotamers were assigned to overlapping bands. In no case were the shifts of the calculated and observed band pairs contradictory. This means that the sign of the observed and calculated *anti*–*gauche* shift were either both positive or both negative. In the cases of overlapping *anti* and *gauche*

fundamentals the calculations gave shifts below 10 cm^{-1} except for the two modes ν_2 and ν_{27}.

If the *anti* rotamer was present in the crystal the interpretations and calculations would be in complete disagreement. Thus, we feel that there is absolutely no doubt that the vanishing bands are *anti*, meaning that the *gauche* conformer remains in the crystal.

The bond moments of the C–Cl and Si–F are much larger than those of the other bonds in CETFS. It is therefore expected that the *anti* conformer with opposite C–Cl and Si–F bonds should have a much smaller dipole moment than *gauche* in which these bonds make approximately a tetrahedral angle. This was supported by the results of the ab initio calculations giving the dipole moments 0.26 and 3.57 D for the *anti* and *gauche* conformers, respectively. In many conformational systems a stabilization of the polar conformer in polar solvents and in the liquid compared to the vapour have been reported [27]. This observation also agrees with the dielectric theory first proposed by Onsager [28].

Therefore, while *anti* is the low energy conformer in the matrices and presumably in the vapour, the stabilization of the polar *gauche* molecule in the liquid leads to *gauche* being the low energy conformer in the latter.

4.3. Assignments

The four antisymmetric and symmetric C–H stretching modes (ν_{17}, ν_1, ν_{18} and ν_2) were assigned to vapour bands from 3006 to 2925 cm^{-1}. Since none of the infrared or Raman bands disappeared in the crystal, all the C–H stretches seemed to have coinciding *anti* and *gauche* bands although for ν_2 the shift was calculated to be 16 cm^{-1}. The infrared and Raman bands around 2900 cm^{-1} were considered to be combination bands or overtones.

Two highly localized CH_2 scissoring modes (ν_3 and ν_4) are assigned to four vapour bands from 1465 to 1400 cm^{-1} constituting two *anti–gauche* pairs. The two CH_2 wagging modes (ν_5 and ν_6) are attributed to the bands at 1313 (*anti*) 1305 (*gauche*) and at 1199 (*anti*) and 1176 cm^{-1} (*gauche*). Intermingled with these, the CH_2 twisting fundamentals of species A″ (ν_{19} and ν_{20}) are found at 1298 (*gauche*), 1280 (*anti*), 1128 (*anti*) and 1121 cm^{-1} (*gauche*). The vapour bands at 1035 and 1025 cm^{-1} and the corresponding Raman bands are assigned to the C–C stretch (ν_7) of the *anti* and *gauche* conformers, respectively.

The two SiF_3 antisymmetric stretching modes (ν_{21} and ν_8) are calculated around 940–930 cm^{-1} with negligible splitting between the *anti* and *gauche* rotamers. The symmetric mode ν_9 at ca. 850 cm^{-1}, however, should have a separation of 12 cm^{-1}. These fundamentals are calculated to be the most intense infrared bands in the spectrum of CETFS, but have weak counterparts in Raman (Tables 3 and 4). The two ν_{21} fundamentals are assigned at 981 cm^{-1} and the ν_8 modes at 972 cm^{-1}, whereas ν_9 is attributed to 879 (*anti*) and 874 cm^{-1} (*gauche*), all these are in good agreement with the predictions. The CH_2 rocking mode ν_{22} is attributed to the vapour bands at 891 (*anti*) and 916 cm^{-1} (*gauche*).

The three vibrational modes: ν_{23} (CH_2 rock), ν_{10} (C–Cl stretch) and ν_{11} (C–Si stretch) give according to the calculations very large *anti–gauche* shifts equal to 55, 52 and 45 cm^{-1}, respectively. As is apparent from Tables 1, 3 and 4 they are attributed to the bands at 779 (*gauche*), 703 (*anti*), 745 (*anti*), 671 (*gauche*) and 703 (*anti*) and 647 cm^{-1} (*gauche*), respectively. The experimental shifts: 76, 74 and 56 cm^{-1} are larger than the predictions. Independent calculations carried out with the MP2/G-31(d) basis set and scaled with 0.9, gave the calculated shifts 84, 84 and 49 cm^{-1} for ν_{23}, ν_{10} and ν_{11}, respectively, giving larger shifts than those observed for ν_{23} and ν_{10}, but too small for ν_{11}. It was found necessary to assume that ν_{11} and ν_{23} of the *anti* conformers overlapped at 703 cm^{-1}, but separate bands at 699 and 695 cm^{-1} were observed in Xe solution. An overlap between different modes is not unlikely for fundamentals of different symmetry species.

The symmetric and anti symmetric $CSiF_3$ deformations were assigned to the bands at 454 (*gauche*) and 426 cm^{-1} (*anti*) for ν_{12} and 364 (*gauche*) and 358 cm^{-1} (*anti*) for ν_{13} in good agreement with the calculated conformer shifts. The two A″ modes involving the $CSiF_3$ twisting fundamental was attributed to overlapping bands at 328 cm^{-1} (ν_{24}). The rocking mode (ν_{25}) was assigned to the pair at 234 (*anti*) and 189 cm^{-1} (*gauche*). The three bending modes: ν_{14}, ν_{15} and ν_{16} are highly mixed according to the PED and each of these are assigned to bands with 48, 17 and 77 cm^{-1} separations between the conformers in reasonable agreement with the calculations.

Finally, the two torsional modes CH_2Cl (ν_{26}) and SiF_3 are tentatively attributed to the vapour bands at 97 and 78 cm^{-1}, respectively, in which the *anti* and *gauche* fundamentals presumably overlap.

The assignments as listed in Tables 1, 3 and 4 agree reasonably well with the predicted infrared and Raman intensities. Also, the observed Raman polarization ratios agree with the A″ modes being polarized and the A″ modes of the *anti* conformer being depolarised, whereas all the *gauche* fundamentals should be polarized. Exceptions are the Raman bands assigned to the *anti* modes ν_{22} and ν_{25} which were given as polarized. The ν_6 fundamental of the *gauche* conformer was noted as a questionable D rather than polarized, but the calculations gave the ρ value 0.72 which is very close to being depolarised.

Acknowledgements

The authors are grateful to Mrs. Anne Horn, Oslo for careful treatment of figures and tables. VA and AG have both received fellowships from *Det Norske Videnskaps-Akademi*, Oslo, Norway.

References

[1] M.A. Qtaitat, J.R. Durig, Spectrochim. Acta 49A (1993) 2139.
[2] M.S. Afifi, G.A. Guirgis, T.A. Mohamed, W.A. Herrebout, J.R. Durig, J. Raman Spectrosc. 25 (1994) 159.
[3] J.R. Durig, G.A. Guirgis, T.A. Mohamed, W.A. Herrebout, M.S. Afifi, J. Mol. Struct. 319 (1994) 109.
[4] H.M. Jensen, P. Klaeboe, V. Aleksa, C.J. Nielsen, G.A. Guirgis, Acta Chem. Scand. 52 (1998) 1359.
[5] H.M. Jensen, P. Klaeboe, V. Aleksa, C.J. Nielsen, G.A. Guirgis, Acta Chem. Scand. 52 (1998) 578.
[6] V. Aleksa, P. Klaeboe, A. Horn, C.J. Nielsen, G.A. Guirgis, J. Mol. Struct. 445 (1998) 161.
[7] V. Aleksa, P. Klaeboe, A. Horn, C.J. Nielsen, G.A. Guirgis, J. Raman Spectrosc. 29 (1998) 627.
[8] V. Aleksa, P. Klaeboe, C.J. Nielsen, V. Tanevska, G.A. Guirgis, Vib. Spectrosc. 17 (1998) 1.
[9] G.A. Guirgis, A. Nilsen, P. Klaeboe, V. Aleksa, C.J. Nielsen, J.R. Durig, J. Mol. Struct. 477 (1997) 410–411.
[10] V. Aleksa, P. Klaeboe, C.J. Nielsen, A. Gruodis, G.A. Guirgis, K. Herzog, R. Salzer, J.R. Durig, J. Raman Spectrosc. 31 (2000) 897.
[11] M. Ernst, K. Schenzel, A. Jähn, K. Hassler, J. Mol. Struct. 412 (1997) 83.
[12] R. Zink, K. Hassler, M. Ramek, Vib. Spectrosc. 18 (1998) 123.
[13] K. Hassler, W. Köll, M. Ernst, Spectrochim. Acta, Part A 53 (1997) 213.
[14] M. Ernst, K. Schenzel, A. Jähn, K. Hassler, J. Mol. Struct. 412 (1997) 83.
[15] K. Hassler, R. Neuböck, Spectrochim. Acta, Part A 49 (1993) 95.
[16] K. Hassler, G. Bauer, Spectrochim. Acta, Part A 43 (1987) 1325.
[17] A. Jähn, K. Schenzel, R. Zink, K. Hassler, J. Raman Spectrosc. 29 (1998) 1055.
[18] V. Aleksa, A. Gruodis, P. Klaeboe, C.J. Nielsen, K. Herzog, R. Salzer, G.A. Guirgis, J.R. Durig, J. Mol. Struct. 482-483 (1999) 563.
[19] F.A. Miller, B.M. Harney, Appl. Spectrosc. 24 (1970) 291.
[20] M.O. Bulanin, J. Mol. Struct. 19 (1973) 59.
[21] B.J. van der Veken, F.R. de Munck, J. Chem. Phys. 9 (1992) 3060.
[22] M.O. Bulanin, J. Mol. Struct. 347 (1995) 73.
[23] W.A. Herrebout, B.J. van der Veken, A. Wang, J.R. Durig, J. Phys. Chem. 99 (1995) 578.
[24] W.A. Herrebout, B.J. van der Veken, J. Phys. Chem. 100 (1996) 9671.
[25] A.J. Barnes, J. Mol. Struct. 113 (1984) 161.
[26] M.J. Frisch, G.W. Trucks, H.B. Schlegel, P.M.W. Gill, B.G. Johnson, M.A. Robb, J.R. Cheeseman, T. Keith, G.A. Petersson, J.A. Montgomery, K. Raghavachari, M.A. Al-Laham, V.G. Zakrzewski, J.V. Ortiz, J.B. Foresman, J. Cioslowski, B.B. Stefanov, A. Nanayakkara, M. Challacombe, C.Y. Peng, P.Y. Ayala, W. Chen, M.W. Wong, J.L. Andres, E.S. Replogle, R. Gomperts, R.L. Martin, D.J. Fox, J.S. Binkley, D.J. Defrees, J. Baker, J.P. Stewart, M. Head-Gordon, C. Gonzalez, J.A. Pople, GAUSSIAN 94, Revision D.2, Gaussian, Inc., Pittsburgh PA, 1995.
[27] R.J. Abraham, E. Bretschneider, in: W.J. Orville-Thomas (Ed.), Internal Rotation in Molecules, Wiley, London, 1874, p. 481.
[28] L. Onsager, J. Am. Chem. Soc. 58 (1936) 1486.